Hopf bifurcation cascade in small-α laser diodes subject to optical feedback

M. Sciamanna,* P. Mégret, and M. Blondel
Service d'Electromagnétisme et de Télécommunications, Faculté Polytechnique de Mons, Boulevard Dolez 31, B-7000 Mons, Belgium
(Received 2 October 2003; published 30 April 2004)

We analyze theoretically the dynamics of a semiconductor laser subject to optical feedback, on the basis of the well-known Lang-Kobayashi equations. Previous investigations on this laser system suggest that a small linewidth enhancement factor (α factor) stabilizes the laser dynamics. By contrast, we unveil here optical feedback induced instabilities which are present for a small value of α but which disappear when α increases above $\alpha \sim 1$. By combining numerical simulations and modern continuation methods for delay-differential equations, we unveil cascades of subcritical and supercritical Hopf bifurcations on the first external-cavity mode (ECM). We unveil for the first time, to our knowledge, the occurrence of subcritical Hopf bifurcation points for intermediate values of the EC length, i.e. close to the boundary between the short and the long EC regimes. They lead to severe laser instabilities such as large intensity and possibly chaotic pulsations. Moreover, these Hopf bifurcation cascades for small values of α are shown to be responsible for different bifurcation scenarios leading to restabilization of the first ECM and to ECM bistability.

DOI: 10.1103/PhysRevE.69.046209 PACS number(s): 05.45.−a, 42.65.Sf

I. INTRODUCTION

Optical feedback in semiconductor lasers, i.e., the reflection of the emitted light into the laser cavity, has attracted the attention of many scientists since more than 20 years, owing to its practical importance as well as its rich and complex nonlinear dynamics (for a review, see, e.g., Petermann [1] and van Tartwijk and Lenstra [2]). An in-depth understanding of the instabilities in laser diodes subject to feedback is indispensable in order to avoid them, or to control and stabilize the laser emission. On the other hand these instabilities may be useful for new applications of laser diodes such as the recently suggested interferometric applications [3], cryptography based on optical chaos [4,5], and also the all-optical generation of high-frequency electrical signals [6–10].

The theoretical modeling of the dynamics of laser diodes with optical feedback is very often based on the Lang-Kobayashi (LK) equations [11]. The LK equations model a single-mode laser diode subject to a weak to moderate optical feedback from a flat, distant mirror. New problems concerned with optical feedback effects in multi-longitudinal mode edge-emitting lasers [12,13] and in vertical-cavity surface-emitting lasers [8,9,14–20] have motivated extensions of the LK equations to more complex rate equations. However, the dynamics of the simple LK equations is still only partially understood and new regimes of instabilities are regularly reported [21,22], which motivate new theoretical investigations in different sets of laser and feedback parameters.

Experiments and numerical simulations have shown that the chaotic instabilities arising in laser diodes subject to delayed feedback emerge from a cascade of bifurcations on the steady states of the laser system, i.e., the so-called external-cavity modes (ECMs) [23]. The ECMs destabilize from a Hopf bifurcation and the emerging time-periodic solution may in turn destabilize to period-doubling regimes or quasi-periodicity and possibly lead to chaotic intensity oscillations. The Hopf bifurcation on ECMs therefore plays an important role since it is often the first bifurcation in the route to more complex optical feedback-induced laser instabilities. Most of the instabilities in the LK equations originate from *supercritical Hopf bifurcations* on ECMs. As we increase a bifurcation parameter, the ECM steady state undergoes a Hopf bifurcation from which emerges a *stable* time-periodic solution. The time-periodic solution grows in amplitude as we increase the bifurcation parameter and may destabilize to more complex laser outputs. Supercritical Hopf bifurcations have been reported, for example, in the cascade of bifurcations leading to chaotic low-frequency fluctuations [23,24], in the route to regular pulse package dynamics [22,25], and recently they were shown to be responsible for the high-frequency harmonic intensity oscillations resulting from a beating between two ECMs [6–10,26].

Very recently, we have shown that *subcritical Hopf bifurcations* are also possible in the LK equations [27], in the so-called short EC regime, i.e., when the EC frequency is much larger than the relaxation oscillation (RO) frequency of the solitary laser diode [6,7]. By contrast to the case of supercritical Hopf bifurcations, the ECM that undergoes a subcritical Hopf bifurcation destabilizes to an *unstable* time-periodic solution. Very often this time-periodic solution stabilizes as we increase the bifurcation parameter, and the laser then exhibits sharp, high-frequency and large intensity pulses [27]. These subcritical Hopf bifurcations are found in a large range of laser and feedback parameters (while remaining in the short EC regime) but they usually disappear and become supercritical as the linewidth enhancement factor α decreases below $\alpha \simeq 1$ (except for particular parameter values) [27,28].

The α factor is one of the fundamental parameters of semiconductor lasers. It is responsible for the enhancement of the laser linewidth, and it affects the frequency chirp, the modulation response, and the effect of optical feedback [29]. In the search for large bandwidth and high-frequency telecommunication systems, there is an increasing need for

*Electronic address: Sciamanna@telecom.fpms.ac.be

small-α laser diodes, which can greatly benefit from the recent developments of quantum dot (QD) active materials [30]. These new interests also motivate further investigations on the dynamical effects of optical feedback in small-α laser diodes. All previous studies on the impact of a small α on the feedback-induced instabilities have reported on stabilization effects. For example, as α decreases, we have the following.

(i) The amount of feedback leading to the onset of the chaotic coherence collapse increases [31,32], i.e., the laser exhibits higher resistance to feedback-induced chaotic instabilities.

(ii) The stability of the maximum gain ECM is significantly improved with respect to the occurrence of chaotic low-frequency fluctuations [33–36].

(iii) The quasiperiodic oscillations which typically accompany the two ECM beatings in short ECs disappear [10].

(iv) The subcritical Hopf bifurcations responsible for large intensity oscillations in short EC convert to much smoother supercritical Hopf bifurcations [27].

In this paper, we show however that a small α factor may also induce instabilities on the ECM steady states, which are not present for conventional, larger values of α. A combination of numerical integration of the LK equations with modern continuation methods for delay-differential equations [37] allows us to report on cascades of subcritical and supercritical Hopf bifurcations on the first ECM. First, we show that the decrease of the α factor is responsible for the appearance of subcritical Hopf bifurcations which, by contrast to previous reports [27], appear for values of the EC length such that the EC frequency is comparable or smaller than the RO frequency of the solitary laser, i.e., in the long EC regime. These subcritical Hopf bifurcations lead to large intensity, possible chaotic pulsations. Second, we show that these Hopf bifurcation cascades may induce restabilization mechanisms of the first ECM and lead to ECM bistability. Finally, our bifurcation study complemented by time traces and spectral analysis allows us to yield some insight into the different physical origins of the reported Hopf-induced instabilities on the first ECM. The dynamical scenarios which we analyze here clearly show that, by contrast to what can be concluded from previous reports (see, e.g., Refs. [31,33–36]), a small α factor may also play a destabilizing role in the dynamics of a laser diode with optical feedback. Our results are therefore thought to give new insight into the Hopf instabilities of delayed laser diodes and also to motivate new experimental studies. Both the subcritical Hopf bifurcations and restabilization mechanisms have typical dynamical signatures which should be easily recognized in experiments.

The plan of our paper is as follows. In Sec. II we remind the reader the Lang-Kobayashi equations and the Hopf bifurcation problem. Our analysis of Hopf bifurcations in delayed lasers with a small α factor is performed in Sec. III. Section IV illustrates the laser instabilities emerging from the Hopf bifurcations shown in Sec. III, on the basis of bifurcation diagrams of the laser intensity. Our conclusions are summarized in Sec. V.

II. HOPF BIFURCATION PROBLEM

Our theoretical analysis is based on the well-known LK equations [11]. In a dimensionless form the LK equations can be written as [38]

$$\frac{dY}{ds} = (1+i\alpha)ZY + \eta\exp(-i\Omega_0\theta)Y(s-\theta), \tag{1}$$

$$T\frac{dZ}{ds} = \overline{P} - Z - (1+2Z)|Y|^2, \tag{2}$$

where Y is the slowly varying amplitude of the electric field and Z is the carrier number in excess with respect to its threshold value. α is the linewidth enhancement factor. The parameter T is defined as the ratio between the carrier lifetime τ_s and the photon lifetime τ_p, i.e., $T \equiv \tau_s/\tau_p$. $\overline{P}$ is a normalized pump term. $\theta \equiv \tau_{ext}/\tau_p$ is the external-cavity round-trip time τ_{ext} normalized by τ_p. $\Omega_0 \equiv \omega_{th}\tau_p$, where ω_{th} is the frequency of the solitary laser at threshold. $\eta \equiv f\tau_p$, where f is the feedback rate.

The Hopf bifurcations on the ECMs can be determined from a standard linear small perturbation analysis on the ECM steady states. We obtain two transcendental equations for η_H, i.e., the critical feedback rate leading to a Hopf bifurcation and the Hopf frequency ω_H. These equations have been derived in several publications (see, e.g., Ref. [38]) and can be written as

$$\begin{aligned} 0 = {} & 2\varepsilon[\overline{P} + \eta_H\cos(\Delta)]\eta_H F_1 Q + 2\omega_H\eta_H F_1 \\ & \times[\eta_H F_2 - \omega_H\cos(\Delta)] - \varepsilon\frac{1+2\overline{P}}{1-2\eta\cos(\Delta)} \\ & \times[\eta_H^2(F_1^2 - F_2^2) + 2\omega_H\eta_H\cos(\Delta)F_2 - \omega_H^2], \end{aligned} \tag{3}$$

$$\begin{aligned} 0 = {} & 2\varepsilon[\overline{P} + \eta_H\cos(\Delta)](\eta_H F_2 Q - \omega_H) - \omega_H \\ & \times[\eta_H^2(F_1^2 - F_2^2) + 2\omega_H\eta_H\cos(\Delta)F_2 - \omega_H^2], \\ & - \varepsilon\frac{1+2\overline{P}}{1-2\eta_H\cos(\Delta)} 2\eta_H F_1[\eta_H F_2 - \omega_H\cos(\Delta)], \end{aligned} \tag{4}$$

where we define

$$\varepsilon \equiv 1/T, \tag{5}$$

$$Q \equiv \cos(\Delta) - \sin(\Delta)\alpha, \tag{6}$$

$$F_1 \equiv \cos(\omega_H\theta) - 1, \tag{7}$$

$$F_2 \equiv -\sin(\omega_H\theta). \tag{8}$$

Because of the time delay in the LK equations, it is hardly possible to solve Eqs. (3) and (4) analytically. Several analytical estimates of the Hopf bifurcations on ECMs have been suggested but they are valid only in a limited range of laser or feedback parameters [6,7,39]. Our procedure to analyze the Hopf bifurcations is therefore the following. We solve numerically the Hopf equations (3) and (4) and analyze the solutions η_H and ω_H as a function of the EC delay time θ. Indeed we are interested in analyzing whether the obtained Hopf bifurcations are limited to the short or to the long EC regimes, which depend on θ. Once the Hopf bifurcation points have been located, we classify these points into

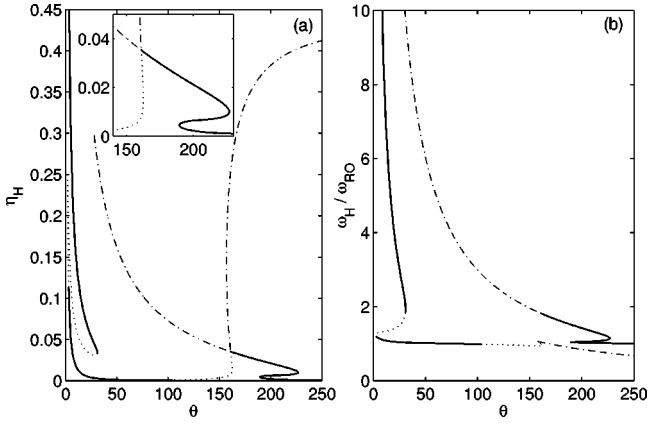

FIG. 1. (a,b) Analysis of the Hopf bifurcation curve in the planes (θ, η_H) and (θ, ω_H/ω_{RO}), respectively. By thick line (dotted line) is shown the part of the Hopf curve corresponding to supercritical (subcritical) Hopf bifurcation points. The dashed-dotted line corresponds to a branch of unstable Hopf bifurcation points. The inset in (a) shows an enlargement of the Hopf curve, in order to better analyze the new subcritical and supercritical Hopf bifurcation points.

either supercritical or subcritical Hopf points, depending on the stability of the time-periodic solution emerging from these Hopf points: super(sub)critical Hopf bifurcations lead to stable (unstable) time-periodic solutions. The stability of the time-periodic solutions emerging from the Hopf bifurcation points has been computed with the use of a recently developed continuation package for delay-differential equations, DDE-BIFTOOL [37]. This continuation package is interesting in that it allows us to analyze the stability of steady states and time-periodic solutions, and to follow branches of steady states and time-periodic solutions irrespective of their stability. In this sense, the use of continuation methods is more powerful than a direct integration of the rate equations since the direct integration only allows us to track the stable attractors.

III. SUBCRITICAL AND SUPERCRITICAL HOPF BIFURCATIONS FOR SMALL α

In Figs. 1(a) and 1(b), we have plotted the solutions η_H and ω_H of Eqs. (3) and (4) as a function of the EC delay time θ and in the case of a small α factor ($\alpha=0.5$). Such a small but nonzero α parameter has been measured, for example, in QD Fabry-Perot laser diodes [30] and has been recently suggested in the context of optical feedback experiments on QD distributed feedback laser diodes [32]. The other parameters are fixed to $\overline{P}=1.155$, $T=1710$, and $\Omega_0\theta=\pi$, which are typical values often used in agreement with optical feedback experiments (see e.g., Ref. [22]). We have checked that our conclusions are valid in a large range of values of laser and feedback parameters providing that the α factor is small. The Hopf frequency ω_H is normalized by the RO frequency $\omega_{RO}\equiv\sqrt{2\overline{P}/T}$. For the parameters we have considered in Fig. 1, the period of the laser relaxation oscillations, $T_{RO}\equiv 2\pi/\omega_{RO}$, corresponds to $T_{RO}\simeq 170$. According to the definition of the short and long EC regimes [6,7], the short (long) EC regime corresponds to values of the EC lengths such that $\theta<(>)170$.

Hopf bifurcations progressively appear on the ECM steady states as we increase the feedback rate η and as new ECM steady states are created. However, we concentrate here on the first Hopf bifurcations that appear on the first ECM steady state. We distinguish different types of Hopf bifurcations. We call stable Hopf bifurcation points the Hopf bifurcations that modify the stability of the ECM steady state, either stabilizing or destabilizing the ECM. These stable Hopf bifurcation points can be either supercritical or subcritical depending on the stability of the emerging time-periodic solution. By solid line (dotted line) is shown the part of the Hopf curve corresponding to supercritical (subcritical) Hopf bifurcation points. By contrast, we call unstable Hopf bifurcations the Hopf bifurcations that do not modify the ECM stability. These Hopf bifurcation points may appear on antimodes, i.e., saddle-type (always unstable) ECMs, but they may also appear on an ECM that has been previously destabilized. The unstable Hopf bifurcation points are plotted with a dashed-dotted line. They are shown for clarity since, as plotted in Fig. 1, a branch of supercritical or subcritical Hopf bifurcation points may convert into a branch of unstable Hopf points.

As shown in Fig. 1(a), a first set of subcritical Hopf bifurcation points (dotted line) appears for very small value of θ ($5\lesssim\theta\lesssim 40$). They appear close to turning points in the S-shaped Hopf curve. These subcritical Hopf bifurcation points, which are typical of the short EC regime and which may also appear for larger values of α, have been extensively studied in Ref. [27]. Interestingly, our analysis of the Hopf bifurcation in small-α laser diodes unveils new Hopf bifurcation cascades and instabilities when $\theta\sim T_{RO}$, i.e., close to the boundary with the long EC regime. First, another set of subcritical Hopf bifurcation points appears for $105\lesssim\theta\lesssim 165$. As shown in the following, these subcritical Hopf bifurcations have dramatic consequences on the laser output and lead to large intensity pulsations and possibly chaotic oscillations. Second, new turning points in the Hopf bifurcation curve appear for these large values of θ. As we shall analyze in more details in the following, these turning points in the Hopf curve are indicative of restabilization mechanisms of the first ECM: as we increase the feedback rate η, a first Hopf bifurcation destabilizes the first ECM but it may restabilize for larger values of η from a second Hopf bifurcation. This second, restabilizing Hopf bifurcation, may be subcritical, as it is the case for $\theta\simeq 162$, or supercritical, as it is the case for $190\lesssim\theta\lesssim 230$. A third important result in our Hopf bifurcation analysis is the situation which appears for $165\lesssim\theta\lesssim 190$: the feedback rate needed to destabilize the first ECM with a Hopf bifurcation is much larger than for smaller or larger values of θ. The first ECM therefore exhibits an increased stability in a rather large region of θ and destabilizes from a supercritical Hopf bifurcation for larger values of η. This supercritical Hopf point belongs to a branch of Hopf bifurcation points that were unstable Hopf points (dashed-dotted line) for smaller values of θ.

The frequency of the Hopf bifurcation is plotted as a function of θ in Fig. 1(b). For most of the values of θ, the first

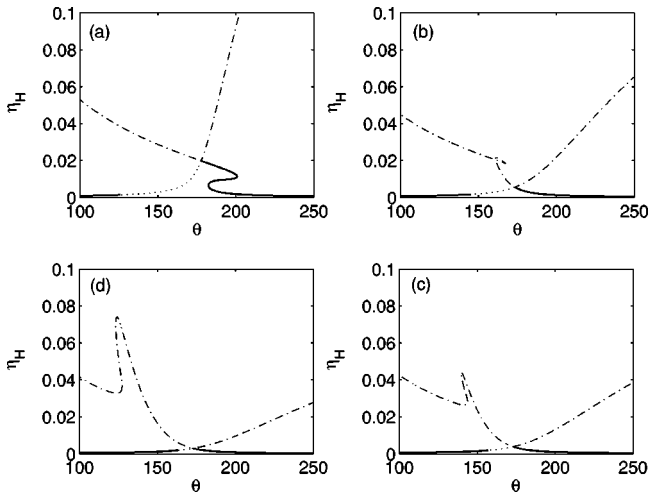

FIG. 2. Analysis of the Hopf bifurcation curve in the plane (θ, η_H) for different values of α: (a) $\alpha=1$, (b) $\alpha=2$, (c) $\alpha=3$, and (d) $\alpha=4$. The other parameters are the same as in Fig. 1.

Hopf bifurcation on the first ECM exhibits a frequency close to the RO frequency. However, for $165\lesssim\theta\lesssim190$, the first ECM destabilizes with a supercritical Hopf bifurcation which, interestingly, exhibits a frequency much larger than the RO frequency. In the previous reports on the dynamics of delayed laser diodes with short EC [6–10,25], the first Hopf bifurcation always occurs with a frequency corresponding to the RO frequency and only the Hopf bifurcations that occur for larger feedback rate η exhibit a larger frequency, close to the EC frequency. Our analysis shows that, while for most of the values of θ the first Hopf bifurcation exhibits indeed the RO frequency, there might be a (small) range of θ where there is no Hopf bifurcation at the RO frequency but only Hopf bifurcations with much higher frequencies.

Our Hopf bifurcation analysis has unveiled instabilities on the first ECM in the case of a small α factor: (1) a large region of subcritical Hopf bifurcations close to the boundary with the long EC regime and (2) the possibility of three consecutive Hopf bifurcations on the same, first ECM. In order to confirm that these instabilities are strongly related to the small value of the α factor we have analyzed the Hopf bifurcation curve as in Fig. 1(a) but for larger values of α; see Fig. 2. The α factor is varied from $\alpha=1$ (a) to $\alpha=4$ (d), all the other parameters remaining equal to those of Fig. 1. If we compare Figs. 2(a)–2(d) with Fig. 1(a), we can conclude that the increase of α has dramatic consequences on the Hopf bifurcations. First, the sequence of two consecutive subcritical Hopf bifurcation points, which was observed close to $\theta=162$ in Fig. 1, is not present anymore when α increases. Still we find subcritical Hopf bifurcation points but in a range of θ that progressively decreases as we increase α, which indicates that these subcritical Hopf bifurcations emerge as a consequence of a small value of α. Second, the sequence of three consecutive supercritical Hopf bifurcations, which was shown in Fig. 1(a) for $190\lesssim\theta\lesssim230$, disappears when α increases above $\alpha=1$. As we increase the α factor the laser dynamics is mostly characterized by a situation in which the first ECM destabilizes with a single supercritical Hopf bifurcation point and then remains unstable whatever the further increase of the feedback rate. The Hopf bifurcation cascade in which the first ECM restabilizes as a result of a subcritical or a supercritical Hopf point is therefore strongly related to a small α factor.

IV. LASER INSTABILITIES EMERGING FROM THE HOPF BIFURCATIONS

We have shown in Sec. III that a small α factor may be responsible for new bifurcation mechanisms on the first ECM. In this section, we shall analyze in more details the laser instabilities that emerge from these Hopf bifurcations. We shall plot the intensity $I\equiv|Y|^2$ of the first ECM steady states and their Hopf bifurcations (symbol $\diamondsuit$) as they appear when we increase the feedback rate η, i.e., a bifurcation diagram for the steady state ECMs. These bifurcation diagrams have been computed with the recently developed continuation method for delay-differential equations, DDE-BIFTOOL [37], since we are interested in a global picture of the instabilities on the first ECMs, including both stable and unstable attractors. By solid (dashed) line is shown the stable (unstable) part of each branch. Hopf bifurcation points are shown with $\diamondsuit$, and the bold $\diamondsuit$ indicate the Hopf bifurcation points that modify the stability of the first ECM. Hopf points with bold $\diamondsuit$ belong in fact to the solid or dotted lines in Fig. 1(a). Each bifurcation diagram of the steady state ECMs will be complemented by another figure, in which we plot the branches of time-periodic solutions emerging from the Hopf bifurcation points. The stability of these time-periodic solutions has been computed from an analysis of the Floquet multipliers, numerically obtained with the package DDE-BIFTOOL. The stable (unstable) parts of the branches of time-periodic solutions are shown in solid (dashed) lines. The time-periodic solutions may destabilize either from a torus bifurcation (symbol *), from a limit point (symbol $\square$), or from a period doubling bifurcation (symbol $\triangle$). Different Secs. IV A–IV D correspond to increasing values of the delay time θ, for which the laser dynamics is qualitatively different.

The instabilities emerging from Hopf bifurcations in the case of a very short EC have been largely discussed in another recent publication [27]. We are interested here in the new set of subcritical and supercritical Hopf bifurcation points, unveiled in Fig. 1, which appear when α is small and for values of θ close to the boundary with the long EC regime ($\theta\simeq T_{RO}=170$).

A. Subcritical Hopf bifurcation, bistability and large intensity oscillations

As shown in Fig. 1(a), when $105\lesssim\theta\lesssim165$ the first ECM destabilizes from a subcritical Hopf bifurcation point. Figures 3(a) and 3(b) illustrate the ECM stability when $\theta=160$. As we increase the feedback rate η from zero, the first ECM destabilizes from a subcritical Hopf bifurcation point and remains unstable if we further increase η. From the subcritical Hopf bifurcation point emerges an unstable branch of time-periodic solution. The branch of time-

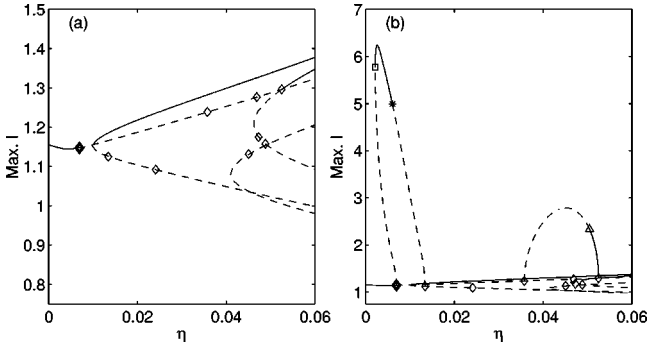

FIG. 3. (a) Bifurcation diagram of the intensity I for the first branches of ECMs as a function of the feedback rate η for $\theta = 160$. The other parameters are the same as in Fig. 1. The Hopf bifurcation points are shown with $\diamond$, and the points indicated with bold $\diamond$ represent the Hopf points corresponding to a change of stability of the first ECM. In (b) are shown some branches of time-periodic solutions emerging from the Hopf bifurcations. The branches of time-periodic solutions are shown in solid (dashed) lines when they are stable (unstable). They destabilize either from a torus bifurcation (*), a limit point ($\square$), or a period doubling bifurcation ($\triangle$).

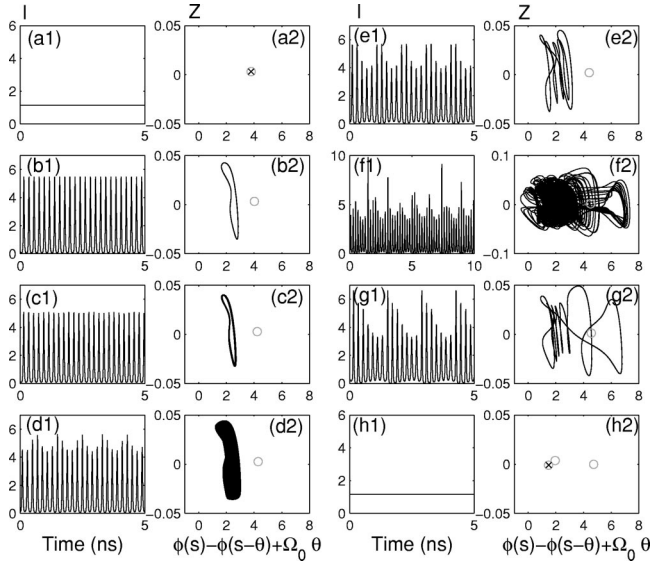

FIG. 4. Large intensity oscillations emerging from a subcritical Hopf bifurcation in delayed laser diode with small-α factor. We plot the time traces of the intensity I and the system trajectory in the phase plane $(\phi(s)-\phi(s-\theta)+\Omega_0\theta,\ Z)$ for increasing values of η: (a1,a2) $\eta=0.004\,00$, (b1,b2) $\eta=0.005\,00$, (c1,c2) $\eta=0.00\,602$, (d1,d2) $\eta=0.006\,40$, (e1,e2) $\eta=0.007\,20$, (f1,f2) $\eta=0.007\,90$, (g1,g2) $\eta=0.008\,30$, and (h1,h2) $\eta=0.010\,00$. The values of the other parameters are the same as in Fig. 3. The circles indicate the ECM steady states.

periodic solution grows in amplitude as we decrease η and coexists with the steady state branch of the first ECM. A bistability between a time-periodic solution and the steady state ECM is therefore observed, as a result of a subcritical Hopf bifurcation. The branch of time-periodic solution stabilizes for small values of η through a limit point ($\square$) and the stable branch of time-periodic solutions destabilizes for larger values of η through a torus bifurcation (*). The subcritical Hopf bifurcation has therefore a dramatic consequence on the laser output. If we increase the feedback rate η from zero, we observe first a steady output power and then, suddenly, a very large intensity oscillation with a maximum of the order of six to seven times the output power of the laser without optical feedback. Moreover, the torus bifurcation indicates that the laser output may exhibit quasiperiodic and possibly chaotic oscillations for slightly larger values of η.

We have analyzed in more details the laser dynamics emerging from the subcritical Hopf bifurcation point. In Fig. 4 we plot the time trace of I together with the system trajectory in the plane $(\phi(s)-\phi(s-\theta)+\Omega_0\theta,\ Z)$, for several increasing values of the feedback rate η. $\phi(s)$ is the phase of the field $Y(s)\equiv|Y|\exp[i\phi(s)-i\Omega_0\theta]$. The function $\phi(s)-\phi(s-\theta)+\Omega_0\theta$ is interesting in that its steady state solution corresponds to the ECM frequency. The continuation package DDE-BIFTOOL only allows us to compute the steady state and time-periodic solutions. We have therefore complemented the continuation study with a direct numerical integration of the LK equations, in order to track also the period-doubling, quasiperiodic and possibly chaotic solutions. For $\eta=0.004\,00$, (a1), (a2), the laser exhibits a steady state solution corresponding to the first ECM. As we increase the feedback rate η, the first ECM undergoes a subcritical Hopf bifurcation and, as shown in Fig. 3(b), the laser then jumps to a large limit cycle attractor, which corresponds to the emission of sharp, large intensity pulses with a frequency close to the RO frequency. This situation is plotted in (b1), (b2) for $\eta=0.005\,00$. As shown in Fig. 3(b), the time-periodic solution emerging from the subcritical Hopf bifurcation destabilizes for larger values of η with a torus bifurcation. Figures 4(c1) and 4(c2) show that for $\eta=0.006\,02$ a small modulation appears on the intensity pulses and the phase space trajectory exhibits a ''noisy'' attractory that results from the combination of the fast pulsating behavior with a slower envelope modulation. For still larger η, the modulation depth has increased and the laser system exhibits a typical quasiperiodic oscillation with a slow modulation of fast intensity pulses; see (d1), (d2) for $\eta=0.006\,40$. As we increase η the window of quasiperiodic oscillations is interspersed with windows of time-periodic oscillations, as shown in (e1), (e2) for $\eta=0.007\,20$. The laser system exhibits a time-periodic pulsating behavior with a period much larger than the fundamental period in (b1), (b2). The limit cycle attractor in the phase space projection (e2) closes on itself after a large number of turns. For $\eta=0.007\,90$, (f1), (f2), the time-periodic solution may bifurcate to a chaoticlike dynamics, in which the intensity exhibits irregular bursts of fast intensity pulses (f1). The system trajectory is very complex in the phase plane (f2) and encircles the first ECM steady state. For larger η, the windows of chaoticlike intensity oscillations are interspersed with windows of time-periodic oscillations, as shown in (g1), (g2) for $\eta=0.00830$. Similar to the cases (e1), (e2), the laser exhibits a time-periodic behavior with irregular bursts of fast intensity pulses. The period is however larger than in (e1), (e2) and the system trajectory now encircles the first ECM and makes

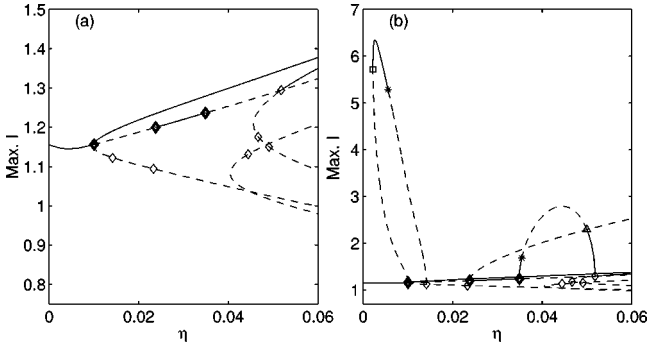

FIG. 5. Same as in Fig. 3 but for $\theta=162$.

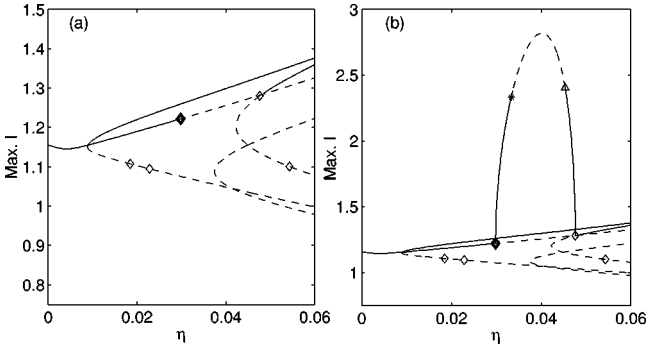

FIG. 6. Same as in Fig. 3 but for $\theta=175$.

several loops before closing on itself. As we increase η further the laser system again locks to a steady-state solution, as shown in (h1), (h2) for $\eta=0.010\,00$, but corresponding to the second ECM. As shown in (h2), a new pair of ECMs (mode-antimode) has been created and the system locks to the mode with the maximum gain (the smaller Z).

The Hopf bifurcation points appearing for larger values of η on the first branch of ECM in Fig. 3 are unstable since the first ECM is already unstable. The branches of time-periodic solutions emerging from these Hopf points are therefore also unstable but they may eventually stabilize as we increase the bifurcation parameter, as shown in Fig. 3(b) close to $\eta=0.035$: a branch of time-periodic solution connects an unstable Hopf point on the first ECM to a supercritical Hopf point on the upper branch of the next ECM, i.e., on the mode branch of the next ECM. The laser dynamics emerging from such an ECM bridge is very different from the one emerging from the subcritical Hopf bifurcation on the first ECM, as will be discussed in more details in Sec. IV D.

B. Re-stabilization of the first ECM with a subcritical Hopf bifurcation

If θ is close to $\theta\simeq 162$, the first ECM may exhibit a sequence of two consecutive subcritical Hopf bifurcation points, as shown in Fig. 1(a). The first ECM destabilizes from a first, subcritical Hopf bifurcation but it may restabilize for larger values of η from a second subcritical Hopf bifurcation point.

This situation is illustrated for $\theta=162$ in Figs. 5(a) and 5(b). Let us first analyze the bifurcation cascade on the first ECM. As we increase η from zero, the first ECM destabilizes from a subcritical Hopf bifurcation as in the case $\theta=160$ but by contrast to this previous case, the first ECM now restabilizes from a second subcritical Hopf bifurcation for a larger feedback rate η. A third supercritical Hopf bifurcation point appears for larger values of η and definitely destabilizes the first ECM steady state. This sequence of three Hopf bifurcations illustrated in Fig. 5(a) emerges from the turning point of the Hopf bifurcation curve when analyzed in the plane (η,θ); see Fig. 1(a). The branch of time-periodic solution emerging from the first subcritical Hopf bifurcation point is very similar to that of the case $\theta=160$. It connects the first subcritical Hopf bifurcation point on the first ECM branch to an unstable Hopf bifurcation located on the antimode branch of the second ECM. The branch of time-periodic solution emerging from the second subcritical Hopf bifurcation point on the first ECM connects to an antimode at much larger values of η [out of the range of η in Fig. 5(b)] and it never stabilizes. Finally, the branch of time-periodic solution emerging from the third supercritical Hopf bifurcation on the first ECM destabilizes as we increase η through a torus bifurcation and restabilizes for larger values of η through an inverse period-doubling bifurcation (symbol $\triangle$). It then connects a supercritical Hopf bifurcation on the mode branch of a next ECM.

If we compare Fig. 5 with Fig. 3, we see that the different cascade of Hopf bifurcations has modified the topology of the bifurcation diagram and has important consequences on the laser dynamics. First, the first ECM can now be restabilized with an inverse (subcritical) Hopf bifurcation. This restabilization mechanism therefore leads to a bistability between this now restabilized first ECM and a second ECM which has appeared stable for smaller values of η, see Fig. 5 for $0.022\lesssim\theta\lesssim 0.035$. Depending on the initial conditions or under presence of noise, the system can therefore exhibit either one steady state or the other one, i.e., either the ECM with the maximum gain (higher intensity) or the now restabilized first ECM with a smaller intensity. Second, the branch of time-periodic solution shown for larger value of η (which connects the first ECM to a next ECM) now exhibits two stable parts close to the two supercritical Hopf bifurcations it connects. As shown in Fig. 2, the small value of the α factor is responsible for this cascade of Hopf bifurcations in a laser diode with optical feedback.

C. High-frequency supercritical Hopf bifurcation on the first ECM

For $\theta\geqslant 165$, the first Hopf bifurcation which destabilizes the first ECM is now supercritical, as shown in Fig. 1(a). Different situations are however possible depending on the values of θ. We first illustrate the bifurcation on the first ECMs when $\theta=175$; see Figs. 6(a) and 6(b).

The first ECM is now stable in a large range of feedback rates η but destabilizes from a supercritical Hopf point when $\eta\simeq 0.03$. Interestingly, as shown in Fig. 1(b), the frequency of this Hopf bifurcation is much larger than the RO and is very close to $1/\theta$. The Hopf bifurcation with a frequency close to the RO frequency, which was the first Hopf bifurcation to destabilize the first ECM in the previous cases of

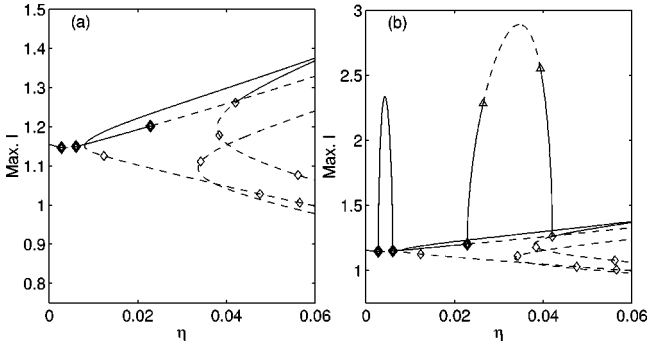

FIG. 7. Same as in Fig. 3 but for $\theta = 195$.

Secs. IV A and IV B, has now disappeared and has been replaced by a Hopf bifurcation at larger value of η and with a higher frequency. It therefore gives a large range of stability to the first ECM. As shown in Fig. 6(b), the branch of time-periodic solution emerging from the supercritical Hopf bifurcation destabilizes through a torus bifurcation but becomes stable for larger feedback rates through an inverse period-doubling bifurcation. It then connects a supercritical Hopf bifurcation on the mode branch of the next ECM. The branch of time-periodic solution shown in Fig. 6(b) is therefore very similar to the branch in Fig. 5(b) which appears close to $\eta = 0.035$, but the first branch of time-periodic solution appearing for small values of η in Fig. 5(b) is not present in Fig. 6(b), as a result of the increased stability for the first ECM.

D. Restabilization of the first ECM with a supercritical Hopf bifurcation

When $190 \lesssim \theta \lesssim 230$, the first ECM exhibits a sequence of three supercritical Hopf bifurcation points as we increase the feedback rate η, as shown in Fig. 1(a). This situation is illustrated for $\theta = 195$ in Figs. 7(a) and 7(b).

As we increase η from zero, the first ECM destabilizes from a supercritical Hopf bifurcation, then restabilizes from a second supercritical Hopf bifurcation, and for larger values of η the first ECM destabilizes from a third supercritical Hopf bifurcation. The branches of time-periodic solutions plotted in Fig. 7(b) show that, interestingly, a completely stable branch of time-periodic solution connects the first ECM to itself for small values of η. As we increase the feedback rate from zero, the laser intensity exhibits first a steady state solution, then a small modulation of intensity appears for increasing η, and the modulation depth increases progressively as we increase η until it reaches a maximum and then decreases again for larger η. The laser intensity then reaches its previous steady state once again. The frequency of the laser intensity modulation is close to the RO frequency, in agreement with the Hopf frequency we computed in Fig. 1(b). A typical time trace corresponding to this time-periodic dynamics is shown in Fig. 8(a). Another branch of time-periodic dynamics is shown in Fig. 7(b) for larger η. This branch emerges from the third Hopf bifurcation and since the Hopf is supercritical, the branch is stable as soon it is created. However it destabilizes through a period-doubling bifurcation for larger values of η. The unstable limit cycle oscillation restabilizes for larger values of η through an inverse period-doubling bifurcation. The intensity dynamics along this branch of time-periodic solutions is illustrated in Fig. 8(b) for $\eta = 0.025$. By contrast to the time-periodic oscillations that appear for a smaller value of η and shown in Fig. 8(a), the frequency of the intensity oscillations is not related to the RO frequency and is about twice the RO frequency.

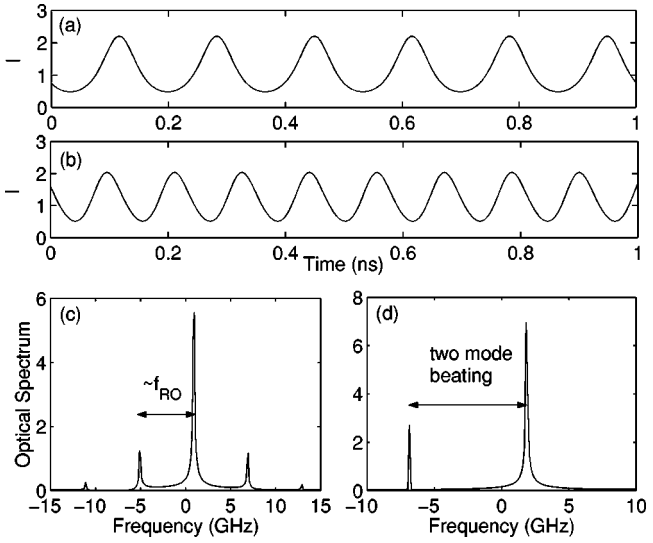

FIG. 8. Time trace of the laser intensity and corresponding optical spectrum for the parameters of Fig. 7 and with (a,c) $\eta = 0.005$ and (b,d) $\eta = 0.025$. In (a,c) is shown a time-periodic intensity dynamics with a frequency close to the RO frequency. It emerges from the destabilization of the first ECM for small value of η and is observed for a value of η along the completely stable branch of time-periodic dynamics that connects the first ECM to itself. In (b,d) is shown a time-periodic intensity dynamics with a frequency larger the RO frequency. It emerges from the destabilization of the first ECM for a larger value of η than in (a) and is observed for a value of η along a bridge of time-periodic solutions that connect the first stable ECM to a second mode (stable ECM).

The physical origin of the harmonic intensity oscillations shown in Figs. 8(a) and 8(b) is very different, as illustrated by the corresponding optical spectra in Figs. 8(c) and 8(d). The optical spectrum shown in (c) corresponds to the dynamics plotted in (a) and which appears from the completely stable branch of time-periodic dynamics that connects the first ECM to itself. A dominant peak appears at the frequency of the first ECM and side peaks are separated from the dominant peak by a frequency span corresponding approximately to the RO frequency. Harmonics of the side peaks are also present in the optical spectrum. The time-periodic dynamics shown in (a) therefore emerges from the destabilization of the first ECM through a Hopf bifurcation, which results in an undamping of the relaxation oscillations. Its physical origin does not involve the other ECMs that appear for larger feedback rate η. By contrast, the optical spectrum in (d), which corresponds to the time-periodic dynamics shown in (b), exhibits only two peaks which are located at the frequencies of two ECMs. This suggests that the time-periodic dynamics shown in (b) physically corresponds to a beating between

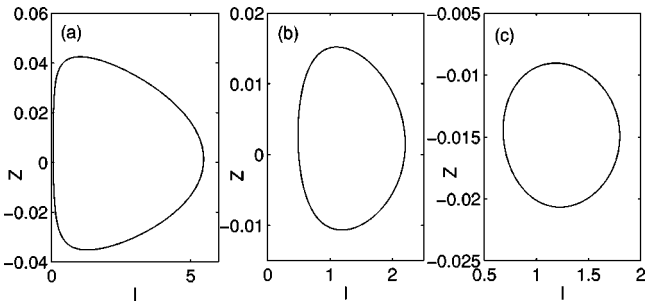

FIG. 9. Trajectory of the laser system in the plane (I, Z), for the limit cycle oscillation shown in Fig. 4(b1), Fig. 8(a), and Fig. 8(b), respectively.

two ECMs. The two beating ECMs correspond to the two-frequency peaks in the optical spectrum. The frequency difference between these two ECMs being much larger than the RO frequency, this explains the faster intensity oscillations in Fig. 8(b) with respect to that in Fig. 8(a). The time-periodic dynamics shown in Fig. 8(b) belongs to what is called a Hopf bifurcation bridge: as shown in Fig. 7(b), a bridge of time-periodic solutions indeed connects two ECMs [24]. The typical case of Hopf bifurcation bridge connects a mode (stable ECM) to an antimode (saddle-type ECM) [6,7,24,26]. It is worth noting that in our case the two beating ECMs are not a mode and an antimode but two stable ECMs (modes). We have recently performed an important analysis of the bridges between ECMs in the short EC regime and found that bridges between two modes are indeed favored by a small α factor [10]. Interestingly, our bifurcation analysis in this paper shows that bridges between modes may also appear when θ is close to the RO period T_{RO}, i.e., in the long EC regime.

The time traces shown in Fig. 4(b1) and Figs. 8(a) and 8(b) are three examples of time-periodic dynamics in the laser system with small value of α, which are of physically and mathematically different origins. The dynamics shown in Fig. 4(b1) emerges from a subcritical Hopf bifurcation on the first ECM, while the dynamics shown in Figs. 8(a) and 8(b) emerge a supercritical Hopf bifurcation on the first ECM. While they both emerge from a supercritical Hopf bifurcation, the dynamics (a) in Fig. 8 is also very different from that shown in (b), since as we have demonstrated one dynamics emerges from a Hopf destabilization of a single ECM, while the second dynamics emerges from a beating between two ECMs that are destabilized by a Hopf bifurcation. The differences between these three dynamics are also very clear when we analyze the phase trajectory, for example, in the plane (I,Z); see Fig. 9. The first case corresponds to the dynamics (b1) in Fig. 4: the dynamics exhibits a large excursion of intensities during each pulse and the trajectory is therefore strongly asymetric in the plane (I, Z). This phase space trajectory is typical of the emission of large intensity pulses. In case (b), which corresponds to the dynamics (a) in Fig. 8, the trajectory is now very close to a symmetric one, hence confirming that the intensity dynamics exhibits harmonic oscillations with well-distributed intensity excursions in the duration of an oscillation. Finally, case (c), which corresponds to the mode beating (b) shown in Fig. 8, exhibits the most symmetric limit cycle trajectory with strongly harmonic intensity oscillations.

V. CONCLUSION

In summary, we have shown that a small α factor may be responsible for various Hopf bifurcation instabilities in laser diodes subject to optical feedback and modeled by the LK equations. For values of the EC delay time θ close to the period of the laser relaxation oscillations (i.e., at the boundary between the short and the long EC regimes), the laser may exhibit subcritical Hopf bifurcations which are associated with strongly pulsating, large intensity, laser outputs. Moreover, the first ECM, which destabilizes from a Hopf bifurcation as we increase the feedback rate η, may restabilize with either a subcritical or a supercritical inverse Hopf bifurcation for larger values of η, hence leading to ECM bistability. These restabilization mechanisms and the subcritical Hopf bifurcations on the first ECM progressively disappear when the α factor increases above $\alpha \sim 1$. Our results therefore show, to our knowledge, for the first time that the decrease of the α factor may also play a destabilizing role in the dynamics of a laser diode subject to optical feedback. Our results are thought to yield new insights into the theoretical aspects of the Hopf bifurcation on ECMs and motivate new experimental studies of small-α laser diodes subject to optical feedback.

ACKNOWLEDGMENTS

The authors acknowledge support from the Fonds National de la Recherche Scientifique (FNRS, Belgium) and the Inter-University Attraction Pole (IAP) program of the Belgian federal government.

[1] K. Petermann, IEEE J. Sel. Top. Quantum Electron. **1**, 480 (1995).
[2] G.H.M. van Tartwijk and D. Lenstra, Quantum Semiclassic. Opt. **7**, 87 (1995).
[3] S. Donati, G. Giuliani, and S. Merlo, IEEE J. Quantum Electron. **31**, 113 (1995).
[4] C. Mirasso, P. Colet, and P. Garcia-Fernandez, IEEE Photonics Technol. Lett. **8**, 299 (1996).
[5] S. Sivaprakasam and K.A. Shore, Opt. Lett. **24**, 466 (1999).
[6] A. Tager and B. Elenkrig, IEEE J. Quantum Electron. **29**, 2886 (1993).
[7] A. Tager and K. Petermann, IEEE J. Quantum Electron. **30**, 1553 (1994).
[8] M. Sciamanna, T. Erneux, F. Rogister, O. Deparis, P. Mégret, and M. Blondel, Phys. Rev. A **65**, 041801(R) (2002).
[9] M. Sciamanna, F. Rogister, O. Deparis, P. Mégret, M. Blondel, and T. Erneux, Opt. Lett. **27**, 261 (2002).
[10] T. Erneux, A. Gavrielides, and M. Sciamanna, Phys. Rev. A **66**,

033809 (2002).
[11] R. Lang and K. Kobayashi, IEEE J. Quantum Electron. **16**, 347 (1980).
[12] D. Sukow, T. Heil, I. Fischer, A. Gavrielides, A. Hohl-AbiChedid, and W. Elsaßer, Phys. Rev. A **60**, 667 (1999).
[13] I. Wallace, D. Yu, R.G. Harrison, and A. Gavrielides, J. Opt. B: Quantum Semiclassical Opt. **2**, 447 (2000).
[14] P. Besnard, F. Robert, M.L. Chares, and G. Stephan, Phys. Rev. A **56**, 3191 (1997).
[15] F. Robert, P. Besnard, M.L. Chares, and G. Stephan, IEEE J. Quantum Electron. **33**, 2231 (1997).
[16] H. Li, A. Hohl, A. Gavrielides, H. Hou, and K. Choquette, Appl. Phys. Lett. **72**, 2355 (1998).
[17] C. Masoller and N.B. Arbaham, Phys. Rev. A **59**, 3021 (1999).
[18] M. Sciamanna, C. Masoller, N.B. Abraham, F. Rogister, P. Mégret, and M. Blondel, J. Opt. Soc. Am. B **20**, 37 (2003).
[19] M. Sciamanna, C. Masoller, F. Rogister, P. Mégret, N.B. Abraham, and M. Blondel, Phys. Rev. A **68**, 015805 (2003).
[20] M. Sciamanna, K. Panajotov, H. Thienpont, I. Veretennicoff, P. Mégret, and M. Blondel, Opt. Lett. **28**, 1543 (2003).
[21] A. Gavrielides, T. Newell, V. Kovanis, R. Harrison, N. Swanston, D. Yu, and W. Lu, Phys. Rev. A **60**, 1577 (1999).
[22] T. Heil, I. Fischer, W. Elsaßer, and A. Gavrielides, Phys. Rev. Lett. **87**, 243901 (2002).
[23] A. Hohl and A. Gavrielides, Phys. Rev. Lett. **82**, 1148 (1999).
[24] D. Pieroux, T. Erneux, B. Haegeman, K. Engelborghs, and D. Roose, Phys. Rev. Lett. **87**, 193901 (2001).
[25] T. Heil, I. Fischer, W. Elsaßer, B. Krauskopf, K. Green, and A. Gavrielides, Phys. Rev. E **67**, 066214 (2003).
[26] D. Sukow, M. Hegg, J. Wright, and A. Gavrielides, Opt. Lett. **27**, 827 (2002).
[27] M. Sciamanna, T. Erneux, A. Gavrielides, V. Kovanis, P. Mégret, and M. Blondel, Proc. SPIE **4986**, 469 (2003).
[28] M. Sciamanna, Ph.D. thesis, Faculté Polytechnique de Mons (FPMs), Belgium, 2004.
[29] M. Osinski and J. Buus, IEEE J. Quantum Electron. **23**, 9 (1987).
[30] T.C. Newell, D.J. Bossert, A. Stintz, B. Fuchs, K.J. Malloy, and L.F. Lester, IEEE Photonics Technol. Lett. **11**, 1527 (1999).
[31] B. Tromborg and J. Mørk, IEEE J. Quantum Electron. **26**, 642 (1990).
[32] H. Su, L. Zhang, A.L. Gray, R. Wang, T.C. Newell, K.J. Malloy, and L.F. Lester, IEEE Photonics Technol. Lett. **15**, 1504 (2003).
[33] T. Heil, I. Fischer, and W. Elsaßer, Phys. Rev. A **60**, 634 (1999).
[34] T. Heil, I. Fischer, and W. Elsasser, J. Opt. B: Quantum Semiclassical Opt. **2**, 413 (2000).
[35] C. Masoller, IEEE J. Quantum Electron. **33**, 796 (1997).
[36] C. Masoller and N.B. Abraham, Phys. Rev. A **57**, 1313 (1998).
[37] K. Engelborghs, T. Luzyanina, and D. Roose, Department of Computer Science, Katholieke Universiteit Leuven, Belgium Technical Report No. TW-330, (Software available at http://www.cs-kuleuven.ac.be/~koen/delay/ddebiftool.shtml) (2000).
[38] P. Alsing, V. Kovanis, A. Gavrielides, and T. Erneux, Phys. Rev. A **53**, 4429 (1996).
[39] T. Erneux, Proc. SPIE **3944**, 588 (2000).